Molecular Crystals and Liquid Crystals

Publication details, including instructions for authors and subscription information:
http://www.tandfonline.com/loi/gmcl20

Dispersion of Organic Dyes in n-Hexadecylamine-Intercalated Vanadium Xerogel Thin Films

Yoshiaki Matsuo [a], Naoya Yamada [a], Tomokazu Fukutsuka [a] & Yosohiro Sugie [a]

[a] Department of Materials Science and Chemistry, Graduate School of Engineering, University of Hyogo, Hyogo, Japan

Version of record first published: 31 Aug 2006

To cite this article: Yoshiaki Matsuo, Naoya Yamada, Tomokazu Fukutsuka & Yosohiro Sugie (2006): Dispersion of Organic Dyes in n-Hexadecylamine-Intercalated Vanadium Xerogel Thin Films, Molecular Crystals and Liquid Crystals, 452:1, 137-158

To link to this article: http://dx.doi.org/10.1080/15421400500377727

Mol. Cryst. Liq. Cryst., Vol. 452, pp. 137–158, 2006

ISSN: 1542-1406 print/1563-5287 online
DOI: 10.1080/15421400500377727

Taylor & Francis
Taylor & Francis Group

Dispersion of Organic Dyes in *n*-Hexadecylamine-Intercalated Vanadium Xerogel Thin Films

Yoshiaki Matsuo
Naoya Yamada
Tomokazu Fukutsuka
Yosohiro Sugie
Department of Materials Science and Chemistry, Graduate School of Engineering, University of Hyogo, Hyogo, Japan

Vanadium xerogels intercalated by n-hexadecylamine were prepared in the presence of hexane. The interlayer spacing of the vanadium xerogel was saturated by n-hexadecylamine at a composition of (n-hexadecylamine)$_{2.2}V_2O_5{\cdot}0.6\ H_2O$. The space between the n-hexadecylamine molecules in the layer was available for adsorption of dye molecules. Large amounts of rhodamine 6G (2.9 wt%), pyrene (1.8 wt%), and p-terphenyl (3.6 wt%) were monomerically intercalated. The I_1/I_3 ratios of the emission peak for pyrene in the intercalation compounds were approximately 0.9, suggesting a nonpolar environment of the interlayer space. The N,N-diethlaminoazobenzene molecules in intercalation compounds were highly confined between n-hexadecylamine molecules.

Keywords: dispersion of dye; intercalation; *n*-hexadecylamine; vanadium xerogel

1. INTRODUCTION

Layered materials have been studied extensively as matrices for photofunctional molecules [1–11]. Applications of these materials include solid dye lasers and nonlinear optics. Clay minerals have been used for photofunctional molecules, introduced via ionic bonding. However, controlling the aggregation state of the introduced molecules is difficult. Recently, two approaches have been proposed to control the aggregation state in clay minerals. One involves the introduction of appropriate substituents to control the distance and

Address correspondence to Yoshiaki Matsuo, Department of Materials Science and Chemistry, Graduate School of Engineering, University of Hyogo, 2167 Shosha, Himeji, Hyogo, 671-2201, Japan. E-mail: ymatsuo@eng.u-hyogo.ac.jp

orientation of the dye molecules in the interlayers of the anionic sheets of the clay [2]. Cationic porphyrins were absorbed on the clay layer surface at a very high density without aggregation; the ratio between the charged sites on the clay and porphyrins reached almost unity. This effect to avoid aggregation has been called the "matching effect." The second approach is to incorporate a third component into the interlayer spacing of clay as a "spacer," together with dye molecules [4–9]. The aggregation of dye molecules or ions can be suppressed in pyrene/cationic surfactant/silica or rhodamine 6G/cationic surfactant/clay hybrid by choosing the appropriate surfactant/dye ratio; light emission from dye monomers was observed in film and powder samples or in aqueous solution. We have reported that aggregation of pyrene and rhodamine B molecules were prevented in graphite oxide thin films containing intercalated *n*-alkyltrimethlyammonium ions or *n*-alkylamines [10,11]. The suppression of aggregation was due to the "spacer" effect of the alkyl chains of amphiphilic molecules or ions. The high content of amphiphilic species in graphite oxide enables greater hydrophobicity of the resulting hydrophobized graphite oxide matrix for easy dispersion in organic solvents, such as chloroform, and for obtaining thin films by casting or spin-coating methods. However, avoiding aggregation of the dye molecules at high loading levels remained difficult. Eliminating aggregation requires reducing the size of the space available between amphiphilic molecules introduced into the layered materials by increasing their numbers or developing new host solids that can accommodate a large number of spacers.

Vanadium oxide xerogel was first synthesized by Lemerle et al. via ion exchange of sodium vanadate [12]. The structure of vanadium oxide xerogel has been determined using the atomic pair distribution function technique [13]. The xerogel slab consists of pairs of single V_2O_5 layers made of pyramidal VO_5 units. Various organic substances, such as pyridine, alkyltrimethylammonium ion, alkylamine, and ammonium ion, have been intercalated into vanadium xerogel at a molecule/V_2O_5 unit ratio of as high as 0.4 [14–22]. These intercalated xerogels are usually prepared by ion exchange. However, the reports on the reaction product between ammonia and vanadium xerogel by spontaneous adsorption ($V_2O_5(NH_4)^+(OH)^- \cdot 0.5H_2O$) indicate that vacant space, allowing more guest molecules in the gallery of xerogel, is still available [23]. Therefore, we synthesized *n*-hexadecylamine-intercalated vanadium xerogels with higher amine contents by solid–solid reaction methods and investigated whether these amine molecules were effective as spacers by measuring emission or absorption spectra of pyrene, *p*-terphenyl, rhodamine 6G, and

N,*N*-diethylaminoazobenzene introduced into *n*-hexadecylamine-intercalated vanadium xerogels.

2. EXPERIMENTAL

Vanadium oxide xerogels (hereafter abbreviated as VXG) were prepared by a sol-gel route as reported previously [12]. A 0.4 M solution of sodium metavanadate was eluted through a column loaded with a proton exchange resin (Rohm and Haas, Amberlite IR124 NA exchanged by HCl). The pale yellow eluent was collected in a glass beaker and allowed to stand at room temperature for evaporation of the water. The resulting solid product was dried at 60°C. The X-ray diffraction pattern of the sample was identical to that reported for VXG ($d_{001} = 1.17$ nm). The water content in VXG was determined from TG datum (Shimadzu TG-50, temperature program: 10°C/min, room temperature to 550°C, under air), and a composition of $V_2O_5 \cdot 1.87H_2O$was obtained. This indicates that this sample contains 1.37 and 0.6 equivalent of weakly and strongly bonded water molecules, respectively.

Intercalation of *n*-hexadecylamine ($C_{16}H_{33}NH_2$; hereafter abbreviated as C16) was performed in a manner similar to that for preparing n-alkylamine-intercalated graphite oxides [10,24–26]. Various amounts of C16 (C16/VXG ratio: 0.25–3.0) were mixed with the vanadium xerogel (ca. 50 mg) in a pestle and the mixtures mechanically ground in the presence of a small amount of hexane (ca. 0.5 ml). After evaporation of the hexane, the resulting products were dried at 60°C overnight. The intercalation compounds (hereafter C16-VXG) obtained were analyzed by infrared (IR) spectroscopy (Nicolet Avatar-360, KBr method), X-ray diffraction (Rigaku Rint-2100, CuKα radiation), X-ray photoelectron spectroscopy (XPS) (Shimadzu ESCA-3400), and thermogravimetric (TG) analysis. The composition of the product was determined by TG and elemental analysis. XPS measurements were performed after drying the sample under vacuum at room temperature overnight. The binding energies observed were corrected based on $Au_{4f}^{7/2}$ electron.

The angle of C16 against the VXG layer was determined by polarized IR spectroscopy [27] and X-ray diffraction. The tilt angle, γ, of the transition moment of the $-CH_2-$ stretching vibration of alkylamine against the VXG layer was calculated from the dichroic ratio, $Ry'x'$, using the following formula for *trans* alkyl chains:

$$Ry'x' = \frac{A_y}{A_x} = \frac{2 - (2/n^2)\sin^2\alpha_1 - [(3/n^2)\sin^2\alpha_1 - 1]\sin^2\gamma}{2 - \sin^2\gamma} \qquad (1)$$

where n indicates the refractive index, α_1 is the incident angle of the polarized light, and 90° was used for the angle of the optical transition moment of the $-CH_2-$ stretching vibration against the VXG layer [27].

Intercalation of dye molecules [rhodamine 6G (R6G); pyrene; *p*-terphenyl; and *N*,*N*-diethylaminoazobenzene] into C16-VXG was performed as follows. A chloroform/ethanol solution (9:1 v/v) containing C16-VXG and dye with various dye/VXG ratios was cast on a quartz substrate hydrophobized by octyltrichlorosilane, resulting in the deposition of dye containing C16-VXG thin-film samples. Transparent and homogeneous films with a thickness of less than 1 μm were obtained.

Thin films containing R6G, pyrene, *p*-terphenyl, or *N*,*N*-diethylaminoazobenzene were analyzed by X-ray diffraction, absorption spectroscopy (Hitachi U-3010), and fluorescence spectroscopy (Hitachi F-2500 with excitation wavelengths of 500 nm for R6G, 330 nm for pyrene, and 285 nm for *p*-terphenyl).

3. RESULTS AND DISCUSSION

3.1. Preparation of C16-VXG

Figure 1 shows the X-ray diffraction patterns of C16-VXG samples with various C16 content. When the initial C16/VXG ratio was 0.25,

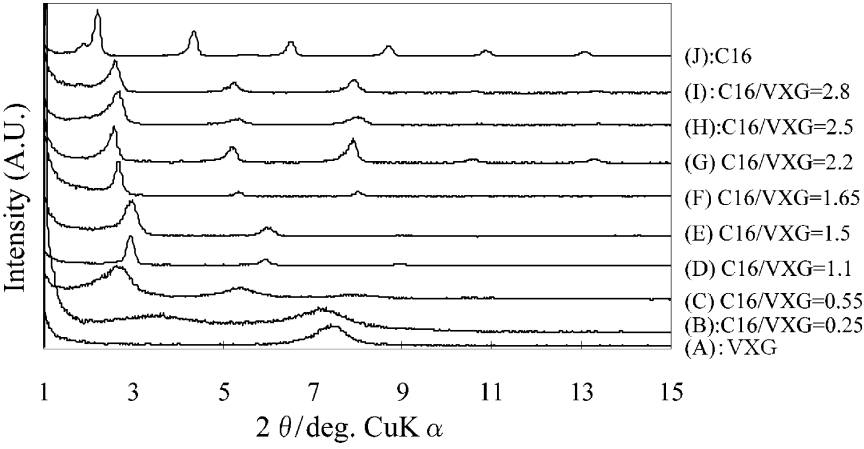

FIGURE 1 X-ray diffraction patterns: (A) vanadium xerogel; (B)–(I) *n*-hexadecylamine-intercalated vanadium xerogel with various nominal C16/V ratios; (J) *n*-hexadecylamine. C16/VXG = (B) 0.25, (C) 0.55, (D) 1.1, (E) 1.5, (F) 1.65, (G) 2.2, (H) 2.5, (I) 2.8.

a diffraction peak due to unreacted V_2O_5 was observed at $2\theta = 7^\circ$, together with a broad peak at $2\theta = 3.7^\circ$. A series of (00 l) diffraction peaks was observed for samples with higher amine contents, indicating intercalation of C16. As C16 content increased, the diffraction peaks shifted slightly to a lower angle until the diffraction angle of (001) peak reached $2\theta = 2.64^\circ$. The calculated interlayer spacing was 3.35 nm, which is similar to that reported for C16-VXG with a C16/VXG ratio of about 0.4 (3.37 nm) [14]. At the same time, the color of the sample changed from reddish brown to green, to yellow, and then to white for samples with nominal C16/VXG ratios larger than 2.2. When the nominal C16/VXG ratio was 3.0, the diffraction peak shifted to a lower angle; however, a small diffraction peak at $2\theta = 1.7^\circ$ appeared, probably due to excess C16 crystals (Fig. 1, J) deposited on the surface of the sample. Therefore, the interlayer spacing of VXG was saturated by C16 for this sample.

Figure 2 shows TG data of various C16-VXG samples, together with those of pristine VXG and C16. A weight decrease, due to the elimination of weakly bonded water, was observed between room temperature and 125°C for samples with nominal C16/VXG ratios smaller than 1.4. This weight decrease was not observed for samples with nominal C16/VXG ratios greater than 1.7, indicating that the 1.37 equivalent of water molecules weakly bonded to the layers did not remain in these samples. Further decreases in weight were observed at 150°C, 250–300°C, and 420–480°C, indicating decomposition of C16. For the sample with a C16/VXG ratio of 3.0, the weight decrease occurring near 70°C was similar to that observed for C16. These results also suggest that excess C16 molecules exist in the sample. After TG measurements, X-ray diffraction measurements confirmed that all samples were converted to crystalline $V_2O_5 \cdot C16$ contents in the intercalation compounds determined from TG data (weight decrease between 150 and 500°C) are summarized in Table 1, assuming that a 0.6 equivalent of water molecules strongly bonded to VXG remain in the sample [14]. However, it was difficult to determine the content of water molecules strongly bonded to VXG on the basis of weight change. Elemental analysis results are shown in Table 1 and agree well with calculated results. The C16/VXG ratios were slightly smaller than the initial ratios, indicating some loss of C16 during reaction.

Figure 3 shows IR spectra of intercalation compounds. As the nominal C16/VXG ratio increases, the absorption peaks at 1016, 775, and 524 cm^{-1} due to terminal V=O, terminal V–O, and bridging O–V–O bondings, respectively [28], became smaller. In contrast, new absorption peaks at 650, 925, and 960 cm^{-1} appeared, together with those

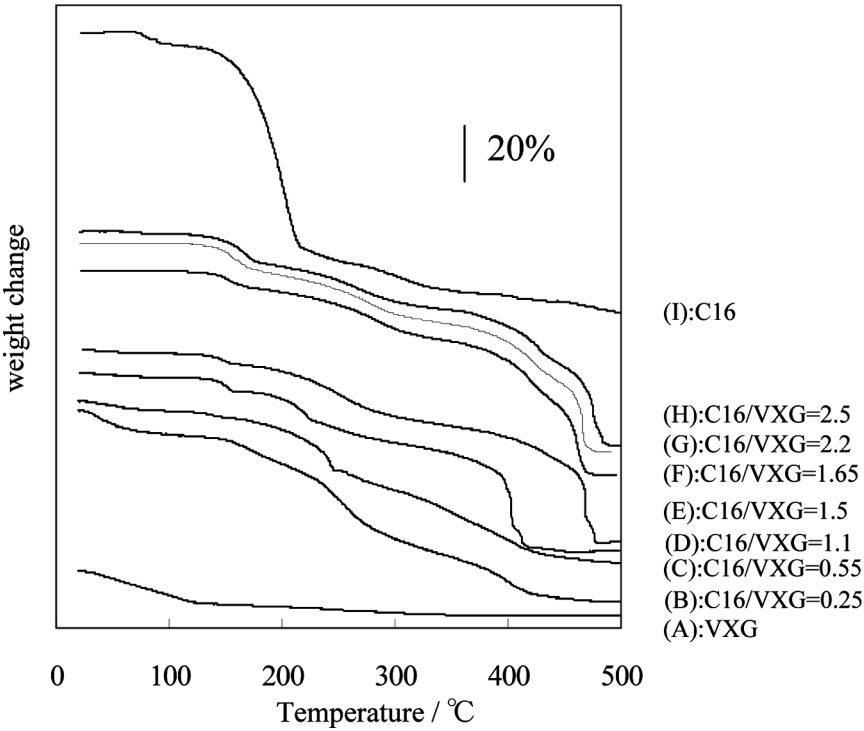

FIGURE 2 TG data: (A) vanadium xerogel; (B)–(H) *n*-hexadecylamine-intercalated vanadium xerogel with various nominal C16/VXG ratios; (I) *n*-hexadecylamine. C16/VXG = (B) 0.25, (C) 0.55, (D) 1.1, (E) 1.5, (F) 1.65, (G) 2.2, (H) 2.5.

due to C16, and increased with C16 content. Peaks at 925 and 960 cm^{-1} could be due to V=O hydrogen-bonded to C16 [29,30]. The relatively sharp peak at 650 cm^{-1} results from the V−O vibration. This peak is similar to that observed for electrochemically reduced VXG cathode of lithium batteries, in which the Li/V ratio is 0.71 [30]. These results suggest that the shift in absorption peaks is due to the elongation of V−O bonds due to reduction of vanadium. When the C16/VXG ratio became 3.0, a small absorption peak at 1310 cm^{-1}, which was unique for C16, appeared, suggesting that excess C16 was deposited on the surface of the C16-VXG. This agrees well with the X-ray diffraction and TG measurements and indicates that maximum C16 content in the interlayer spacing of VXG sample is 2.2 per VXG (the sample with a nominal C16/VXG ratio of 2.8). The peaks due to the asymmetric vibration mode of methylene $[-(CH_2)_n-]$ were observed at

TABLE 1 Composition of Vanadium Xerogel and *n*-Hexadecylamine-Intercalated Vanadium Xerogels

Nominal C16/V_2O_5	Color	Found (elemental analysis)			Composition	Calculated		
		Carbon	Hydrogen	Nitrogen		Carbon	Hydrogen	Nitrogen
0	orange	—	—	—	$V_2O_5 \cdot 1.87H_2O$			
0.55	dark green	*	*	*	$(C16)_{0.45}V_2O_5 \cdot 1.71H_2O$	26.91	5.97	1.96
1.1	dark green	42.14	7.81	3.04	$(C16)_{0.88}V_2O_5 \cdot 1.51H_2O$	40.10	8.03	2.93
1.5	green	*	*	*	$(C16)_{0.18}V_2O_5 \cdot 1.43H_2O$	46.05	8.98	3.36
1.65	green	49.89	9.12	3.64	$(C16)_{1.49}V_2O_5 \cdot 1.04H_2O$	51.10	9.69	3.73
2.2	yellowish white	55.22	10.23	3.95	$(C16)_{1.94}V_2O_5 \cdot 0.6H_2O$	56.40	10.47	4.11
2.5	white	57.48	10.49	4.15	$(C16)_{2.10}V_2O_5 \cdot 0.6H_2O$	57.70	10.69	4.20
2.8	white	*	*	*	$(C16)_{2.22}V_2O_5 \cdot 0.6H_2O$	58.57	10.84	4.27

Note: *, not determined.

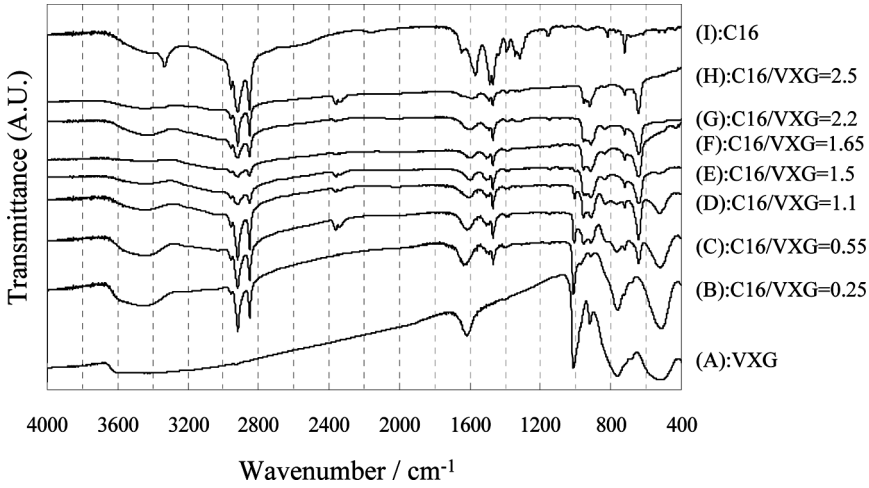

FIGURE 3 IR spectra: (A) vanadium xerogel; (B)–(H) *n*-hexadecylamine-intercalated vanadium xerogel with various nominal C16/VXG ratios; (I) *n*-hexadecylamine. C16/VXG = (B) 0.25, (C) 0.55, (D) 1.1, (E) 1.5, (F) 1.65, (G) 2.2, (H) 2.5.

2917 cm^{-1}, indicating an all-*trans* conformation of the alkyl chain as in the case of crystalline n-alkanes [31–33]. This conformation results from the dense packing of the C16 molecules in the gallery of the VXG layer.

Figure 4 shows the $V_{2p}^{3/2}$, N_{1s}, and O_{1s} XPS data for VXG and various C16-VXG samples. The deconvoluted $V_{2p}^{3/2}$ peaks of VXG and C16-VXG with a nominal C16/VXG ratio of 0.55 are also shown. In the $V_{2p}^{3/2}$ region, a relatively broad peak around 517 eV, consisting of two peaks at 517.2 eV and 516.2 eV, was observed for the pristine VXG. These peaks can be attributed to V^{5+} and V^{4+} ions, respectively [17,33–36]. The ratio of the two peaks indicated that nearly 90% of the vanadium atoms of VXG were in the +5 state. As C16 content increased in VXG, the peak became somewhat broader and the intensity of the peak at lower binding energy increased until the C16/VXG ratio reached 1.1. The deconvoluted $V_{2p}^{3/2}$ peaks of C16-VXG with a nominal C16/VXG ratio of 0.55 suggest that most vanadium atoms are reduced to the +4 state by the introduction of C16. The amount of vanadium atoms in the +5 state decreased to 55% for samples with C16/VXG ratios larger than 1.1, indicating almost half of the vanadium atoms were reduced by introducing C16 molecules, and this condition did not change for samples with higher C16 content. The

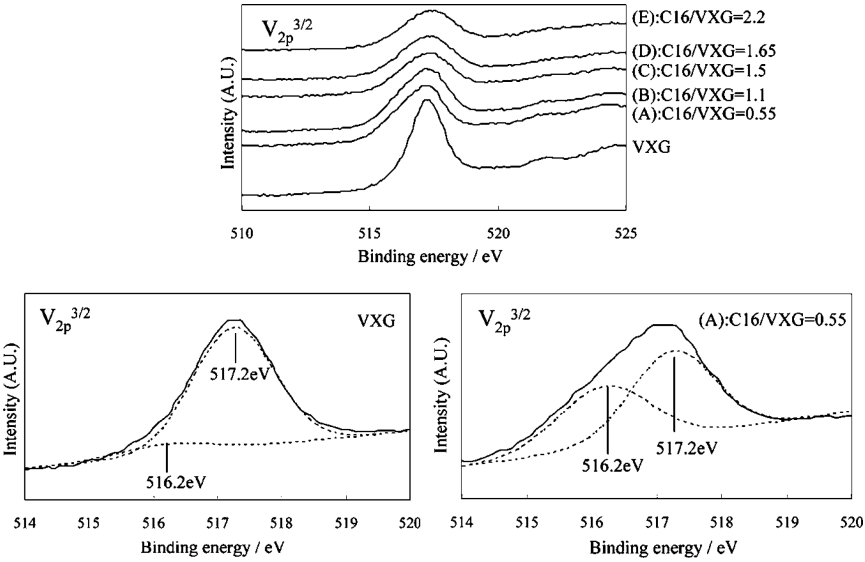

FIGURE 4 $V_{2p}^{3/2}$, N_{1s}, and O_{1s} XPS spectra of (A): VXG (vanadium xerogel) and *n*-hexadecylamine-intercalated vanadium xerogel with nominal C16/VXG VXG ratios of (B) 0.55, (C) 1.1, (D) 1.5, (E) 1.65, and (F) 2.2, along with the deconvoluted $V_{2p}^{3/2}$ spectra of VXG and (B), O_{1s} spectra of VXG and (D), and N_{1s} spectrum of (F).

mechanism of VXG reduction to such a high extent is not well understood; however, mechanical energy supplied during grinding of the VXG-C16 mixture may enhance the reduction of VXG by C16. In contrast, in the N_{1s} region, a broad peak that separated into two peaks at 401.7 eV and 399.9 eV was observed, probably due to hydrogen-bonded amino and ammonium groups, respectively. These peaks appear in 3-aminopropylethoxysilane adsorbed from toluene onto the hydroxylated surface of fused quartz by amino groups [37]. Therefore, the 401.7 eV peak is caused by formation of an ammonium ion ($C_{16}H_{33}NH_2 + H_2O \rightarrow C_{16}H_{33}NH_3^+ + -OH-V{=}O$) as reported for alkylamine-intercalated mixed niobyl-vanadyl phosphate [38]. As C16 content increased, the peak at lower binding energy increased, suggesting an increase in weakly bonded neutral C16 molecules. On the other hand, the O_{1s} region contains three peaks due to oxygen bonded to vanadium, OH groups, and water molecules [17], as shown in the deconvoluted peaks. In this study, these peaks were observed at 530.3, 531.8, and 532.7 eV, respectively. As C16 content increased, the relative intensity of the peak at 531.8 eV increased whereas that

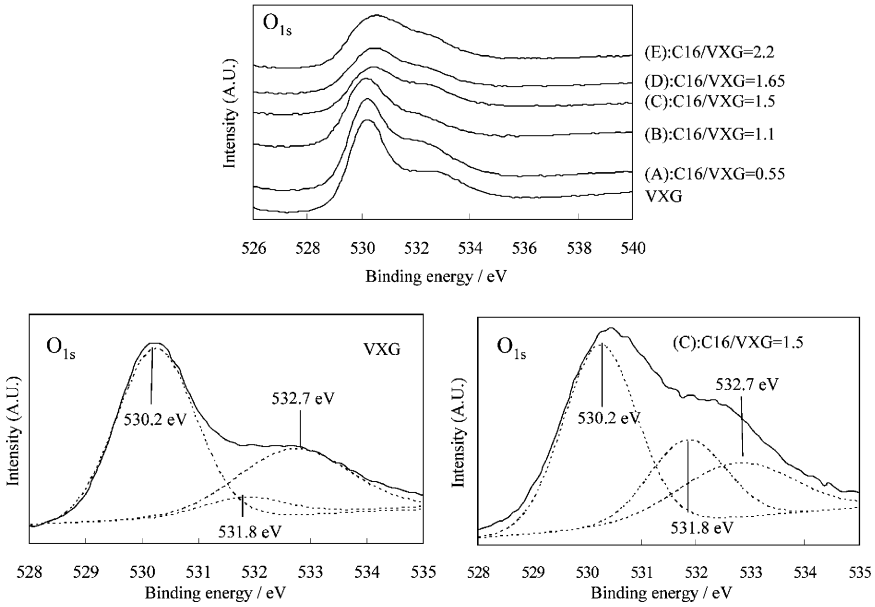

FIGURE 4 Continued.

at 532.7 eV decreased. When the nominal C16/VXG ratio became greater than 1.1, the relative intensity became nearly constant.

Figure 5 shows the absorption spectra of VXG and C16/VXG films with various nominal C16/VXG ratios. The C16/VXG film was nearly colorless, whereas the VXG films prepared from a water suspension were orange. Two absorption peaks at 373 and 247 nm appeared in VXG, with the former peak due to the $O \rightarrow V^V$ CT transition band at V=O bonding [39]. The peaks were broadened in the sample with a nominal C16/VXG ratio of 0.55 and a new, small peak at 310 nm appeared. It has been reported that the peak at 373 nm disappeared upon electrochemical reduction [40–43]. When the nominal C16/VXG ratio was greater than 1.1, a similar spectrum was obtained containing two peaks at 305 and 230 nm, suggesting perturbation in V=O by the introduction of C16 when the C16/VXG ratio was 0.4 to 1. Further addition of C16 into VXG did not affect the chemical environment of the vanadium. Absorption below 600 nm decreased significantly, as expected from the color change of the samples. This characteristic is a benefit for application of these substances as a matrix of dye molecules.

These spectroscopic data indicate that reaction of VXG with C16 occurs in two stages. During the first stage, water content decreased

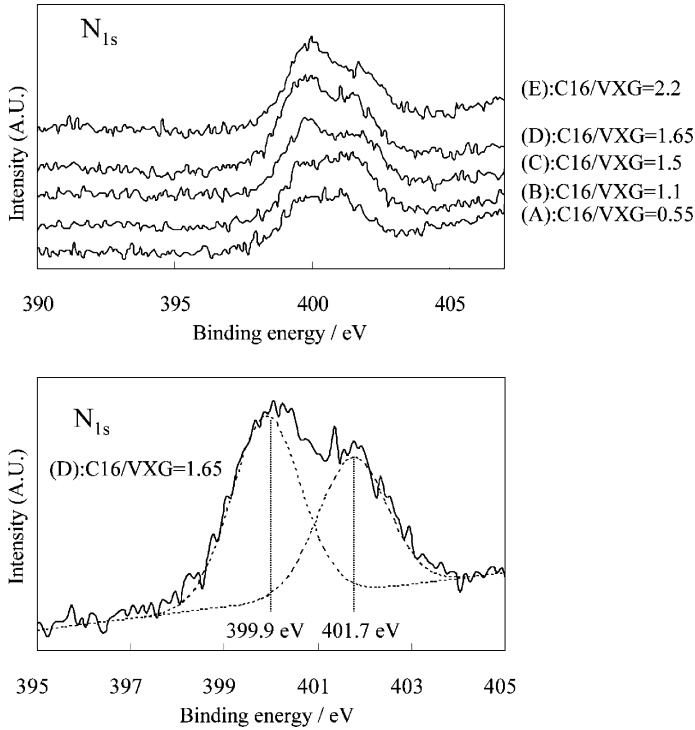

FIGURE 4 Continued.

accompanied by reduction of vanadium from +5 to +4 and formation of ammonium; therefore, weakly bonded water molecules must be substituted by C16 molecules. XPS data suggested that nearly half of the vanadium atoms were reduced in this stage of reaction. During the second stage, little spectroscopic change was observed for samples with actual C16/VXG ratios greater than 1; it is likely that the C16 molecules are accommodated in the gallery of VXG between C16 molecules without affecting the chemical environment of vanadium. The interlayer space was saturated by C16 molecules when the actual C16/VXG ratio reached 2.2, a value greater than can be predicted on the basis of the area requirement of C16 molecules ($0.186\,nm^2$) and the available surface per vanadium calculated from the lattice constant of VXG [12] ($0.127\,nm^2$), assuming perpendicular orientation of C16 to the VXG layer. The co-intercalation of excess amine in the layer has been observed for C16-intercalated birnessite-type manganese oxide [43]. Two explanations can be provided for the excess C16 molecules in the gallery of VXG. The C16 molecules may be

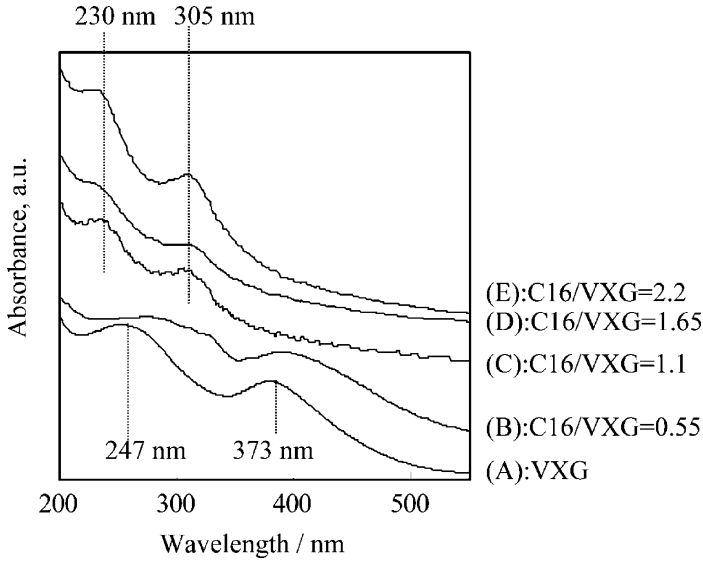

FIGURE 5 UV-vis spectra: (A) vanadium xerogel and C16-VXG films with nominal C16/VXG ratios of (B) 0.55, (C) 1.1, (D) 1.65, (E) 2.2.

deposited on the C16-VXG phase without crystallization or, alternatively, the orientation of VO_5 pyramids may change to accommodate a greater density of C16 molecules in the VXG layer gallery. The change in the infrared absorption peaks, especially in the region of V−O vibrations, for samples with actual C16/VXG ratios between 0.4 and 1 supports the latter possibility. Further structural analysis is necessary to determine the correct explanation for the observed phenomenon. The addition of C16 molecules greatly increased the solubility of the resulting samples in organic solvents. Further increase in C16 (nominal C16/V ratio greater than 2.8) resulted in the deposition of C16 molecules on the surface of C16-VXG. The C16 content in VXG was much higher than in C16-intercalated VXG prepared by reaction between ammonium salts of C16 and VXG (C16/VXG ratio of 0.3–0.4) [14].

3.2. Orientation of Alkylamines in VXG Layers

Two orientations of alkyl chains in the gallery of VXG are possible based on the X-ray diffraction pattern of C16-VXG with a nominal C16/VXG ratio of 2.5. One is an interdigitated monolayer orientation

and the other is a more inclined bilayer orientation. An all-*trans* orientation of $-CH_2-$ was suggested by IR data. Assuming that the thickness of VXG without water molecules in the interlayer is 0.87 nm (1.15–0.28 nm) [44], the thickness of intercalated species was calculated to be 2.48 nm. Based on the size of C16 ($1.27 \times 16 + 0.28 = 2.31$ nm), 90° and 33.1° of inclined angles of alkyl chains against VXG layer were obtained for interdigitated monolayer and bilayer orientations, respectively. Figure 6 shows the dichroic ratio of the asymmetric vibration mode of methylene $-(CH_2)_n-$ groups, which decreased as incident angle increased. This indicates that the tilt angle, γ, is less than 54.7° because the dichroic ratio increases with refractive index, n, if the tilt angle is higher than this value. Therefore, a bilayer orientation of alkyl chain is excluded, although the refractive index remains unknown. The experimental data agreed well with Eq. (1), using a refractive index of $n = 1.5$ and tilt angle of $\gamma = 0°$ (interdigitated monolayer) as shown Fig. 6 (solid line). The refractive index was much smaller than that reported for crystalline vanadium oxide ($n = 1.9$–2.4) [45,46]; however, it was comparable to that of organic materials. This is reasonable considering a large part of the sample consisted of organic material. These results indicate that the orientation of the alkyl chains in the gallery of VXG is an interdigitated monolayer for samples with high amine content, as proposed for C16-VXG with low C16 content [14]. Considering the all-trans conformation of alkyl chains of C16-VXG with nominal C16/VXG greater than 1.1, these also possess interdigitated monolayer orientation, and the smaller interlayer spacing observed in

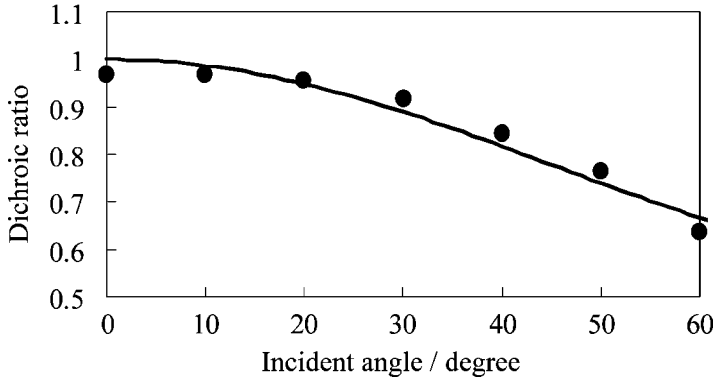

FIGURE 6 Dichroic ratio of the absorption of methylene group of C16-VXG as a function of incident angle. Solid line indicates data calculated using Eq. (1).

Fig. 1 was ascribed to the smaller inclined angle of alkyl chains against VXG layer.

3.3. Dispersion of Dye Molecules in C16-VXGs

In sections 3.3 and 3.4, dispersion and confinement of dye molecules in C16-VXG with various C16 contents was investigated. To know the effect of C16 content in VXG in detail, samples with different C16 contents from those listed in Table 1 were also synthesized by changing nominal C16/VXG ratios. Hereafter, the host materials are abbreviated as $(C16)_x$VXG using x value as the actual C16 content in VXG. The samples with the x values of 1.2, 1.35, 1.5, 1.65, 1.8, 1.9, and 2.1 were used here. Figure 7 shows emission spectra of R6G intercalated $(C16)_{1.65}$VXG samples with various R6G/VXG ratios. At low R6G/VXG ratios, an emission peak was observed at 538 nm as in dilute ethanol solution (535 nm). The peak position was constant regardless of the dye content; therefore, R6G molecules must be dispersed in $(C16)_{1.65}$VXG in a monomeric form. The emission peak shifted to longer wavelengths when the R6G/VXG ratio reached 0.065, indicating aggregation of the R6G molecules. Thus, the maximum monomeric R6G content in the interlayer spacing of $(C16)_{1.65}$VXG is between R6G/VXG = 0.05 and 0.065. The emission peak due to the R6G monomer gradually shifted from 544 nm for $(C16)_{1.2}$VXG to 536 nm for $(C16)_{1.8}$VXG as C16 content increased. These peaks appeared at shorter wavelengths than those observed for R6G adsorbed on silica (555 nm) [47], R6G intercalated in laponite

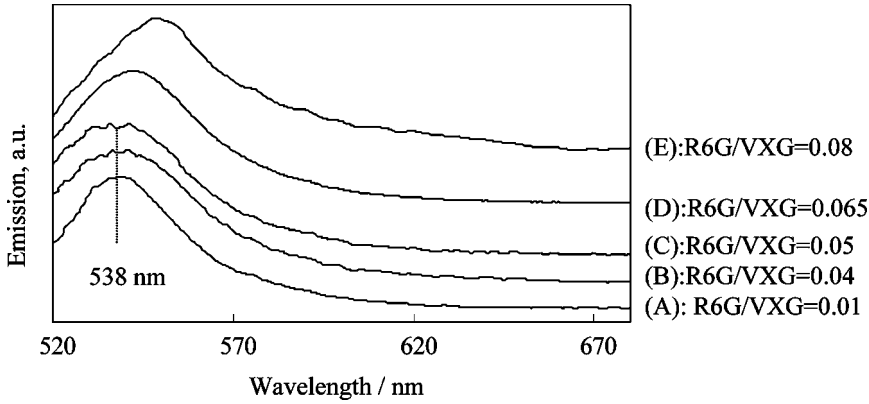

FIGURE 7 Emission spectra of R6G in $(C16)_{1.65}$VXG with R6G/VXG ratios of (A) 0.01, (B) 0.04, (C) 0.05, (D) 0.065, (E) 0.08.

clay (546 nm) [48], and R6G intercalated in sodium montmorillonite (555 nm) [49]. This blue shift in the emission peak also was observed for rhodamine B molecules introduced in graphite oxide hydrophobized with perfluoroalkyltrichlorosilane and *n*-hexadecylamine, when the *n*-hexadecylamine content increased [50]. We propose that this blue shift is due to the less-polar environment surrounding rhodamine B molecules in the intercalation compounds. Here, R6G molecules also are located in a less-polar environment surrounded by alkyl chains, and the π^* excited state was not stabilized as well as in polar media. !Therefore, the energy difference between the π and π^* states increased beyond that found in more polar media and, accordingly, the emission peak shifted to shorter wavelengths. The R6G/VXG ratio that did not result in Rh6G aggregation corresponds to 2.9 wt% of dye molecules in VXG, which is comparable to that observed for rhodamine B in graphite oxide hydrophobized by C16 [10]. In X-ray diffraction patterns of $(C16)_{1.8}$VXGs containing R6G with R6G/V ratio of 0.05 and 0.065, a series of diffraction peaks was observed at $2\theta = 2.64$, 5.1, and 8.1°, with an interlayer spacing of 3.35 nm. This indicates that R6G molecules were intercalated into the space between alkylamines oriented perpendicular to the VXG layer.

Figure 8 shows the emission spectra of pyrene-$(C16)_{1.8}$VXG at pyrene/VXG ratio of 0.02 and 0.03. A series of peaks was observed near 380 nm, attributed to pyrene monomer. As pyrene content increased, a broad peak at 450 nm due to pyrene excimer was observed. Therefore, pyrene molecules also were introduced monomerically at low

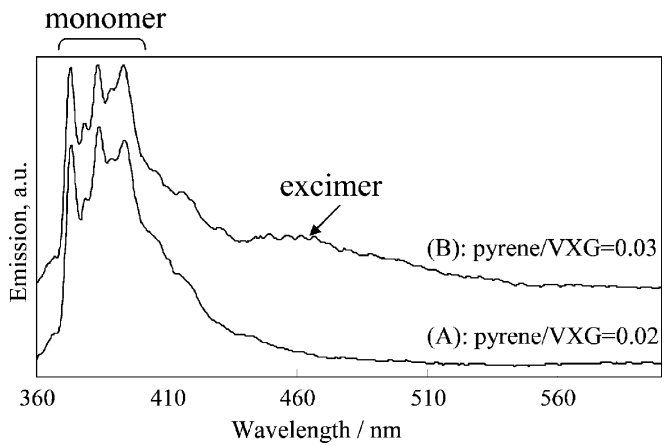

FIGURE 8 Emission spectra of pyrene in $(C16)_{1.65}$VXG with pyrene/VXG ratios of (A) 0.02 and (B) 0.03.

pyrene concentration, whereas aggregation occurred at higher pyrene content. The intensity ratio (I_1/I_3) of the peak at 373 nm to that at 384 nm was approximately 0.9, increasing slightly from 0.82 to 0.92 as the C16 content of C16-VXG increased. The I_1/I_3 ratio is a good indication of the environment surrounding pyrene and was similar to that observed for pyrene dissolved in alcohol with a long alkyl chain [51]. The I_1/I_3 ratio was much smaller than that observed for pyrene introduced into layered silica hydrophobized by alkyltrimethylammonium ion with long alkyl chain lengths (1.25–1.47) [6], which are quite high and normally observed in polar media. This difference may be due to co-adsorbed water molecules, indicating that polar water molecules are excluded from area surrounding the pyrene molecules in the C16-VXG samples as was suggested from the peak position of R6G shown previously. The interlayer spacing determined from X-ray diffraction data was unchanged from that of pristine $(C16)_{1.8}$VXG at lower pyrene content. The maximum monomeric pyrene content introduced in the interlayer spacing was between 0.05 and 0.06.

Figure 9 shows emission spectra of *p*-terphenyl-$(C16)_{1.8}$VXG at various *p*-terphenyl/VXG ratios. As observed for the other two dyes, at lower *p*-terphenyl concentrations, two emission peaks at 323 and 337 nm indicating *p*-terphenyl monomer were observed. Two new peaks at 352 and 372 nm, due to low-dimensional crystals or aggregates of *p*-terphenyl [52], appeared at higher *p*-terphenyl concentrations. No change in interlayer spacing was observed by X-ray diffraction analysis. The maximum monomeric *p*-terphenyl content in the interlayer spacing was between 0.10 and 0.13, somewhat higher than those observed for the other two dyes.

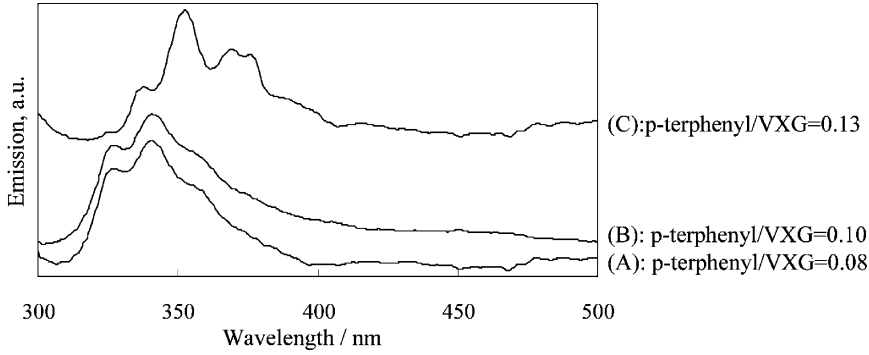

FIGURE 9 Emission spectra of *p*-terphenyl in $(C16)_{1.65}$VXG with *p*-terphenyl ratios of (A) 0.08, (B) 0.10, (C) 0.13.

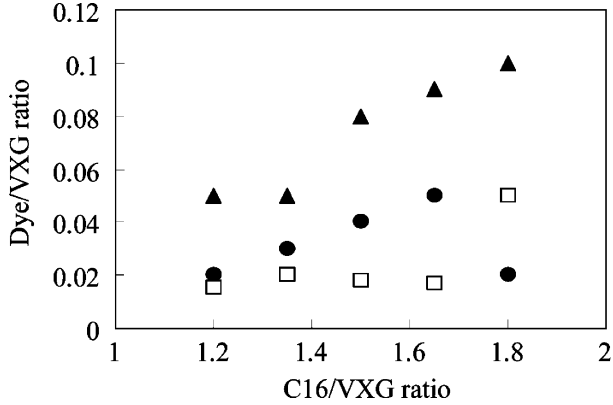

FIGURE 10 Maximum dye content in $(C16)_xVXG$ as a function of C16 content. ●: rhodamine 6G, □: pyrene, and ▲: *p*-terphenyl.

Figure 10 shows the maximum monomeric dye content in C16-VXG samples as a function of C16 content in VXG. In general, maximum dye content increased with C16 content of VXG. As the number of C16 molecules in the VXG layer increased, it is reasonable to assume that the size of the adsorption site for the dye molecules decreases. Therefore, an increase in maximum monomeric dye content in the intercalation compounds is counterintuitive. One possible explanation is that the additional C16 molecules prevent aggregation of R6G due to the "spacer" effect, although at lower C16 contents, the size of most adsorption sites for a single dye molecule were too large to allow dispersion in a monomeric state. The abrupt decrease of maximum monomeric dye content observed only for $(C16)_{1.8}VXG$ with bulky R6G molecules could be due to a decrease in the number of sites between C16 molecules suitable for R6G because of C16 occupation. The maximum monomeric content increased for the smaller pyrene and *p*-terphenyl molecules because the spacer effect was operational for these molecules.

The maximum content of the long and narrow *p*-terphenyl was greater than those for the other dyes. Several factors can determine how many dye molecules can be introduced as monomers, including size of the adsorption site and strength of dye–dye and dye–alkylamine attractive interactions. As discussed previously, the size of the adsorption site is larger than the molecular size of the dyes; thus, the size effect does not explain why the maximum monomeric *p*-terphenyl content was larger than that of the others. In contrast, the interaction between the dye molecules and alkylamines in VXG is

hydrophobic and depends on the contact area of the dye molecules with alkylamine. The difference in the strength of the attractive interactions between dye–dye and dye–amine is small for long and narrow *p*-terphenyl molecules because of the greater contact area of the dye with the amine when compared with that for pyrene or R6G. Therefore, *p*-terphenyl molecules were more easily dispersed between amines than pyrene and R6G. It is very interesting that the dispersion behavior of dye molecules changed significantly with the alkylamine content in VXG and the sizes of them.

3.4. Confinement of *N,N*-Diethylaminoazobenzene in C16/VXGs

Figure 11 shows UV-vis spectra of *N*,*N*-diethylaminoazobenzene-intercalated $(C16)_{1.9}VXG$ with various *N*,*N*-diethylaminoazobenzene content. A broad peak, consisting of two peaks at 430 nm and 466 nm, occurred in spectra of samples with low dye content. The interlayer spacing for these samples calculated from X-ray diffraction data was similar to that for $(C16)_{1.9}VXG$ without dye molecules, suggesting that the dye molecules were introduced into empty space between C16 molecules. As dye content increased (dye/V ratio > 0.13), the peak at 466 nm became dominant and shifted to higher wavelengths, indicating aggregation of dye molecules.

Figure 12 shows UV-vis spectra of *N*,*N*-diethylaminoazobenzene-intercalated $(C16)_{1.9}VXG$ with a dye/V ratio of 0.1, together with those

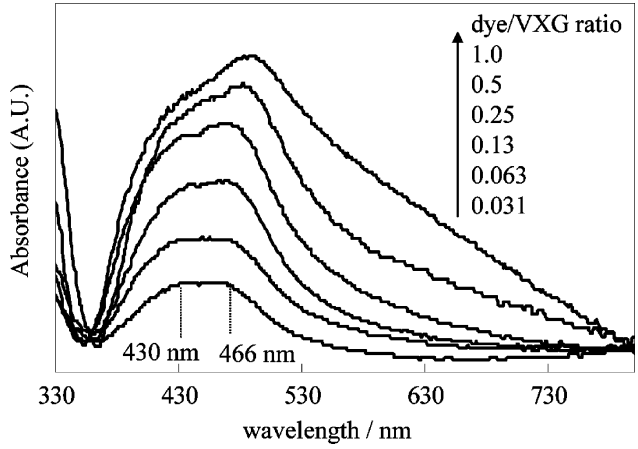

FIGURE 11 Absorption spectra of *N*,*N*-diethylaminoazobenzene intercalated into C16-VXG with various dye vanadium ratios.

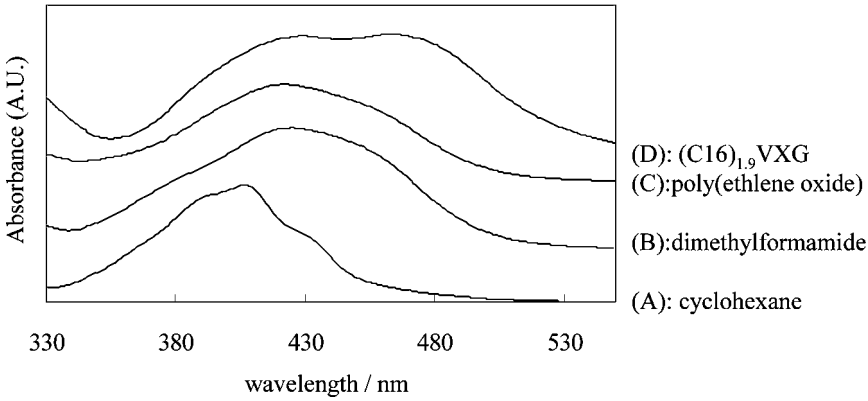

FIGURE 12 Absorption spectra of *N*,*N*-diethylaminoazobenzene in various media: (A) cyclohexane, (B) dimethylformamide, (C) poly(ethylene oxide) (2 wt%), $(C16)_{1.9}$VXG (dye/V ratio of 0.13).

in poly(ethylene oxide) (PEO), dimethylformamide (DMF), and cyclohexane (as examples of polymeric, polar, and nonpolar solvents, respectively). Three peaks were observed at 430, 405, and 391 nm, due to $0 \rightarrow 0$, $0 \rightarrow 1$, and $0 \rightarrow 2\pi_1 - \pi_1^*$ transitions, respectively [53]. Similar spectra were observed for PEO and DMF, in which the relative intensity of the peak due to the $0 \rightarrow 2$ transition diminished, whereas that of $0 \rightarrow 0$ became larger. Simultaneously, peak positions shifted to higher wavelengths. In contrast, the $0 \rightarrow 2$ transition scarcely occurred for the C16-VXG sample [as shown in Fig. 12, D] and absorption peaks occurred at considerably higher wavelengths. The $0 \rightarrow 0$ transition is due to a vibronic transition from the ground state to the planar excited state; the $0 \rightarrow 1$ transition represents the N = N stretching vibronic transition between the ground state and a planar vibrational excited state and the $0 \rightarrow 2$ transition is attributed to the torsional vibronic transition around C_6H_5–N(=) bonds in the excited state. In polar solvents such as DMF, the torsional motion of the benzene ring is highly restricted because the dye molecules are confined in a solvent cage. The greater intensity of the $0 \rightarrow 0$ transition in C16-VXG samples than in polar DMF or PEO suggests that the *N*,*N*-diethylaminoazobenzene molecules in C16-VXG samples are highly confined. The *trans*-to-*cis* photoisomerization of azobenzene molecules has been reported in organophilic tetrasilicic mica [54,55]. However, in the intercalation compounds presented here, photoisomerization did not occur. This lack of azobenzene photoresponse is due to confined

nature of the molecules. The spectra of *N*,*N*-diethylaminoazobenzene molecules in C16-VXG with various C16/VXG ratios are comparable, indicating that the *N*,*N*-diethylaminoazobenzene molecules are similarly confined, although the density of C16 molecules was higher for samples with higher C16 content because the interlayer spacing of these samples did not differ. The number of C16 molecules surrounding the rod-shaped *N*,*N*-diethylaminoazobenzene molecules did not increase with C16 content, thereby confining the *N*,*N*-diethylaminoazobenzene molecules.

The photophysical properties of dye molecules introduced into C16-VXG samples shown in sections 3.3 and 3.4 indicate that the size of the space available between C16 molecules in C16/VXG can be controlled by adjusting the C16 content and that the introduced molecules are highly confined as in polar solvents.

4. CONCLUSIONS

The reaction between *n*-hexadecylamine and vanadium xerogel in the presence of a small amount of hexane provides new vanadium xerogels intercalated by *n*-hexadecylamines. X-ray diffraction, FT-IR, TG, and UV-vis data indicate that saturated intercalation compounds without bulk hexadecylamine have a formula of $(C16)_{2.2}V_2O_5{\cdot}0.6H_2O$. The intercalation of *n*-hexadecylamine into VXG occurred in two steps: substitution of weakly bonded water molecules by C16 molecules, accompanied by the coordination of C16 molecules to V=O, and introduction of *n*-hexadecylamine between existing C16 molecules via hydrophobic interactions. Addition of more C16 molecules resulted in the deposition of C16 crystals on the surface of C16-VXG. C16 alkyl chains possess an all-*trans* configuration and are located in the VXG gallery as interdigitated monolayers when C16 content was high. Maximum monomeric dye content in C16-VXG could be controlled by adjusting the C16 content in VXG, due to the spacer effect of C16 molecules and large numbers of dye molecules dispersed as monomers in the gallery of VXG. The maximum monomeric content of long and narrow *p*-terphenyl was larger than those of pyrene and R6G. The I_1/I_3 ratio of pyrene in the intercalation compounds indicated that the interlayer spacing was highly hydrophobic. The absorption peak ratios due to $0\rightarrow0$ and $0\rightarrow1$ transitions of *N*,*N*-diethlaminoazobenzene molecules intercalated into C16-VXG samples were larger than those in dimethylformamide, indicating that *N*,*N*-diethlaminoazobenzene molecules are highly confined in the nanospace of C16-VXG.

ACKNOWLEDGMENTS

The authors thank to Masayuki Kawaguchi of Osaka Electro-Communication University for his assistance with the XPS measurements.

REFERENCES

[1] Ogawa, M. & Kuroda, K. (1997). *Bull. Chem. Soc. Jpn.*, *70*, 2593.
[2] Takagi, S., Shimada, T., Eguchi, M., Yui, T., Yoshida, H., Tryk, D. A., & Inoue, H. (2002). *Langmuir*, *18*, 2265.
[3] Shiragami, T., Nabeshima, K., Matsumoto, J., Yasuda, M., & Inoue, H. (2003). *Chem. Lett.*, *32*, 484.
[4] Ogawa, M., Aono, T., Kuroda, K., & Kato, C. (1993). *Langmuir*, *9*, 1529.
[5] Ogawa, M., Wada, T., Kuroda, K., & Kato, C. (1995). *Langmuir*, *11*, 4598.
[6] Ogawa, M., Igarashi, T., & Kuroda, K. (1998). *Chem. Mater.*, *10*, 1382.
[7] Hayakawa, K., Fujiyama, N., & Satake, I. (2001). *Stud. Surface. Sci. Catal.*, *132*, 813.
[8] Sasai, R., Fujita, T., Iyi, N., Itoh, H., & Takagi, K. (2002). *Langmuir*, *18*, 6578.
[9] Sasai, R., Iyi, N., Fujita, T., & Takagi, K. (2003). *Chem. Lett.*, *32*, 550.
[10] Matsuo, Y., Hatase, K., & Sugie, Y. (1999). *Chem. Commun.*, *43*.
[11] Matsuo, Y., Fukutsuka, T., & Sugie, Y. (2003). *Chem. Lett.*, *32*, *1109*.
[12] Lemerle, J., Nejem, L., & Lefebvre, J. (1980). *J. Inorg. Nucl. Chem.*, *42*, 17.
[13] Petkov, V., Trikalitis, P. N., Bozin, E. S., Bilinge, S. J. L., Vogt, T., & Kanatzidis, M. G. (2002). *J. Am. Chem. Soc.*, *124*, 10157.
[14] Bouhaouss, A. & Aldebert, P. (1983). *Mat. Res. Bull.*, *19*, 47.
[15] Chirayil, T., Zavalij, P. Y., & Whittingham, M. S. (1998). *Chem. Mater.*, *10*, 2629.
[16] Casal, B., Ruiz-Hitzky, E., Crespin, M., Tinet, D., & Galván, J. C. (1986). *J. Chem. Soc. Faraday Trans. 1*, *82*, 1597.
[17] Casal, B., Ruiz-Hitzky, E., Crespin, M., Tinet, D., & Galván, J. C. (1989). *J. Chem. Soc. Faraday Trans. 1*, *85*, 4167.
[18] Liu, P., Moudrakovski, I. L., Liu, J., & Sayari, A. (1997). *Chem. Mater.*, *9*, 2513.
[19] Rojas-Cervantes, M. L., Casal, B., Aranda, P., Savirón, M., Galván, J. C., & Ruiz-Hitzky, E. (2001). *Colloid Poym. Sci.*, *279*, 990.
[20] Trikalitis, P. N., Petkov, V., & Kanatzidis, M. G. (2003). *Chem. Mater.*, *15*, 3337.
[21] Soga, N. & Senna, M. (1993). *Solid State Ionics*, *63–65*, 471.
[22] Gimenes, M. A., Profeti, L. P. R., Lassali, T. A. F., Graeff, C. F., & Oliveira, O. H. P. (2001). *Langmuir*, *17*, 1975.
[23] Ruiz-Hitzky, E. & Casal, B. (1986). *J. Chem. Soc., Faraday Trans. 1*, *82*, 1597.
[24] Matsuo, Y., Fukunaga, T., Tokura, N., Fukutsuka, T., & Sugie, Y. (2004). *Trans. Mat. Res. Soc. Jpn.*, *29*, 3219.
[25] Matsuo, Y., Watanabe, K., Fukutsuka, T., & Sugie, Y. (2003). *Carbon*, *41*, 1545.
[26] Matsuo, Y., Fukunaga, T., Fukutsuka, T., & Sugie, Y. (2002). *Mol. Cryst. Liq. Cryst.*, *386*, 45.
[27] Akutsu, H., Kyogoku, Y., Nakahara, H., & Fukuda, K. (1975). *Chem. Phys. Lipids*, *15*, 222.
[28] Van Damme, H., Letellier, M., Tinet, D., Kihal, B., & Erre, R. (1984). *Mat. Res. Bull.*, *19*, 1635.
[29] Hardcastle, F. D. & Wachs, I. E. (1991). *J. Phys. Chem.*, *95*, 5031.

[30] Miura, T., Sugiura, E., Kishi, T., & Nagai, T. (1988). *Denki Kagaku Oyobi Kogyobutsurikagaku* (presently *Electrochemistry*), *56*, 413.
[31] MacPhail, R. A., Strauss, H. L., Snyder, R. G., & Elliger, C. A. (1984). *J. Phys. Chem.*, *88*, 334.
[32] Venkataraman, N. V. & Vasudevan, S. (2001). *J. Phys. Chem. B*, *105*, 1805.
[33] Vaia, R. A., Teukolsky, R. K., & Giannelis, E. P. (1994). *Chem. Mater.*, *6*, 1017.
[34] Moulde, J. F., Stickle, W. F., Sobol, P. E., & Bomben, K. D. (1995). *Handbook of X-ray photoelectron spectroscopy, physical electronic*, Eden Praire, MN.
[35] Bondarenka, V., Grebinskij, S., Kaciulis, S., Mattogno, G., Mickvicius, S., Tvardauskas, H., Volkov, V., & Zakharova, G. J. (2001). *Electron Spectr.*, *120*, 131.
[36] Garía-Ponce, A. L., Moreno-Real L., & López, J. (1990). *J. Solid State Chem.*, *87*, 20.
[37] Kowalczyk, D., Slomkowski, S., Chehimi, M., & Delmar, M. (1996). *Int. J. Adhension Adhesives*, *16*, 227.
[38] Barbero, B. P., Cadús, L. E., & Hilaire, L. (2003). *Appl. Catal. A*, *246*, 237.
[39] Ackermans, B., Schoonheydt, R. A., & Ruiz-Hitzky, E. (1996). *J. Chem. Soc., Faraday Trans. 1*, *92*, 4479.
[40] Whalen, K. & Villemure, G. (1996). *J. Electroanal. Chem.*, *411*, 43.
[41] Cogan, S. F., Nguyen, N. M., Perrotti, S. J., & Rugh, R. D. (1989). *J. Appl. Phys.*, *66*, 1333.
[42] Benmoussa, M., Outzourhit, A., Jourdani, R., Bennouna, A., & Ameziane, E. L. (2003). *Active and Passive Elec. Comp.*, *26*, 245.
[43] Wortham, E., Bonnet, B., Jones, D. J., Rozère, J., & Burns, G. R. (2004). *J. Mater. Chem.*, *14*, 121.
[44] Legendre, J.-J. & Livage, J. J. (2004). *Colloid Interface Sci.*, *94*, 75.
[45] Krishna, M. G. & Bhattacharya, A. K. (1997). *Vacuum*, *48*, 879.
[46] Ramana, C. V., Hussain, O. M., Uthanna, E., & Naidu, B. S. (1998). *Opt. Mater.*, *10*, 101.
[47] del Monte, F., Mackenzie, J., & Levi, D. (2000). *Langmuir*, *16*, 7377.
[48] Martínez, V., Lopéz Arbeloa, F., Bañuelos Prieto, J., Arbeloa Lopéz, T., & Lopéz Arbeloa, I. (2001). *Langmuir*, *20*, 5709.
[49] Sasai, R., Iyi, N., Taketoshi, T., Lopéz Arbeloa, F., Martínez, V., Takagi, K., & Itoh, H. (2004). *Langmuir*, *20*, 4715.
[50] Matsuo, Y., Fukunaga, T., Fukutsuka, T., & Sugie, Y. (2004). *Chem. Lett.*, *33*, 1432.
[51] Kalyanasundaram, K. & Thomas, J. K. (1977). *J. Am. Chem. Soc.*, *99*, 2039.
[52] Dutta, A. K. & Mistra, T. N. (1994). *J. Pal. J. Phys. Chem.*, *98*, 12844.
[53] Mustroph, H. (1991). *Dyes and Pigments*, *15*, 129.
[54] Fujita, T., Iyi, N., & Klapyta, Z. (1998). *Mater. Res. Bull.*, *33*, 1693.
[55] Fujita, T., Iyi, N., & Klapyta, Z. (2001). *Mater. Res. Bull.*, *36*, 557.